Monthly Notices of the ROYAL ASTRONOMICAL SOCIETY

MNRAS **552,** 1–13 (2026)
Advance Access publication 2026 September 3

https://doi.org/10.1093/mnras/stag1664

Contributions and timing characteristics of Forbush decreases from substructures of interacting ICMEs

Zavkiddin Mirtoshev [1★], Wageesh Mishra [2★] and Nandita Srivastava [3★]

[1]*Department of Nuclear Physics and Astronomy, Samarkand State University, 15, University boulevard, Samarkand 140104, Uzbekistan*
[2]*Indian Institute of Astrophysics, II Block, Koramangala, Bengaluru 560034, India*
[3]*Udaipur Solar Observatory, Physical Research Laboratory, Badi Road, Udaipur 313001, India*

Accepted 2026 August 27. Received 2026 August 26; in original form 2026 April 1

ABSTRACT

Forbush decreases (FDs) are short-term reductions in galactic cosmic ray (CR) intensity associated with interplanetary coronal mass ejections (ICMEs). We analyze a diverse sample of eight interacting ICME events (2010–2015), spanning merged and separate ejecta, with and without an interaction region (IR), and interactions at different heliocentric distances, to examine how ICME substructures modulate CR intensity and to inter-compare the events for patterns linked to their configuration. Using *in situ* solar wind and magnetic field data with CR intensity at 10 GV from the FEID data base, we identified multistep FD profiles, with substructure boundaries from the Richardson & Cane ICME catalogue (timing uncertainty ±1 h). FD amplitudes range from ∼2.5 to ∼5.8 per cent, showing only a moderate, non-robust correlation with geomagnetic storm intensity. A three-step profile, not possible for an isolated single-ejecta ICME, occurs in two events, while four others show two ejecta-related steps with weak or absent sheath; yet amplitudes, decline rates, and recovery durations (2–4 d) fall within isolated-ICME ranges, so interacting events differ mainly in substructure number and sequencing. FD onset relative to shock arrival varies, with early onsets up to ∼11 h occurring preferentially for interactions closer to the Sun, based on a small sample. A lag of 1–17 h separates the peak field and FD minimum, reflecting cross-field diffusion in the sheath or diffusion-expansion in the ejecta. The dominant CR-modulating substructure varies between the preceding ICME, following ICME, or IR. Given the limited sample, results are illustrative, and a larger matched sample is needed to confirm them.

Key words: Sun: corona – Sun: coronal mass ejections (CMEs) – solar–terrestrial relations – cosmic rays.

1 INTRODUCTION

Forbush decreases (FDs) are short-term depressions in cosmic ray (CR) intensity, typically lasting from a few hours to several days, often occurring as a result of large-scale solar wind disturbances, such as interplanetary coronal mass ejections (ICMEs) and their associated substructures (S. E. Forbush 1937; J. A. Simpson 1954; H. V. Cane 2000; M. Dumbović et al. 2020; A. Papaioannou et al. 2020; M. Janvier et al. 2021; N. S. Shlyk et al. 2022). ICMEs typically consist of a forward shock (when the ejecta speed exceeds the ambient magnetosonic speed), a turbulent sheath region, and a magnetic ejecta that often exhibits a flux-rope-like structure (L. Burlaga et al. 1981; I. G. Richardson & H. V. Cane 2010; E. Kilpua, H. E. J. Koskinen & T. I. Pulkkinen 2017; M. Temmer et al. 2023). Each of these substructures contributes to the modulation of CR through distinct physical mechanisms and results in the commonly observed multi- or two-step FD profile (H. V. Cane et al. 1994; J. L. Freiherr von Forstner et al. 2020).

The sheath region, located downstream of the shock and upstream of the magnetic ejecta, is characterized by large magnetic field variability and enhanced plasma compression. These conditions suppress CR transport through strong pitch-angle scattering and reduced cross-field diffusion over an extended spatial scale (G. Wibberenz et al. 1998; K. P. Arunbabu et al. 2015). In contrast, the magnetic ejecta is characterized by a strong, smoothly rotating magnetic field and relatively low turbulence. The ordered flux-rope topology limits cross-field transport into its interior, and the resulting CR modulation can be described by diffusion-expansion models such as ForbMod (M. Dumbović et al. 2018). The combined influence of these substructures produces an initial decrease of CR intensity associated with the sheath, followed by a subsequent or sustained modulation over the ejecta duration (H. V. Cane et al. 1994; J. L. Freiherr von Forstner et al. 2020).

Superposed epoch and event-based analyses have shown a clear correspondence between ICME substructure boundaries and the temporal evolution of FD profiles, indicating that the sheath and ejecta contribute differently to the depth, rate, and recovery of CR depression (J. J. Masías-Meza et al. 2016; M. Janvier et al. 2021; E. E. Davies, R. M. Winslow & D. J. Lawrence 2023a). The relative contribution of these regions, however, varies from

★ E-mail: zmirtoshev@gmail.com (ZM); m.wageesh30@gmail.com (WM); nandita@prl.res.in (NS)

© The Author(s) 2026.
Published by Oxford University Press on behalf of Royal Astronomical Society. This is an Open Access article distributed under the terms of the Creative Commons Attribution License (https://creativecommons.org/licenses/by/4.0/), which permits unrestricted reuse, distribution, and reproduction in any medium, provided the original work is properly cited.

Downloaded from academic.oup.com/mnras/article/552/1/stag1664/8785133 by Indian Institute of Astrophysics user on 19 October 2026

event to event: fast ICMEs with strong shocks are often sheath-dominated, whereas well-organized flux ropes with strong magnetic fields tend to produce ejecta-driven decreases (H. V. Cane 2000; A. P. Jordan et al. 2011; I. G. Richardson & H. V. Cane 2011; K. P. Arunbabu et al. 2013). Moreover, the magnetic field within the ejecta has been shown to correlate more strongly with FD amplitude than magnetic fluctuations, and significant FDs can occur even in the absence of a well-defined sheath (A. Bhaskar, P. Subramanian & G. Vichare 2016; M. Janvier et al. 2021). While these results are largely based on isolated ICMEs, their applicability to interacting CME events remains unclear, where multiple shocks, merged sheaths, and compressed ejecta may jointly control the rate and depth of FD.

The role of ICME magnetic structure in CR modulation has also been examined in recent observational and modeling studies. E. E. Davies et al. (2023b) showed that the magnitude and temporal evolution of FDs are largely independent of open or closed magnetic field-line topology, and instead depend more strongly on solar wind speed, internal magnetic field structure, and ICME expansion. FD characteristics are also found to evolve with heliocentric distance as ICME substructures expand and weaken during propagation (G. Kinoshita et al. 2026). Numerical simulations further indicate that magnetic flux ropes can produce CR anisotropies in addition to flux attenuation (A. Lara et al. 2024), while diffusion-expansion models such as ForbMod successfully reproduce flux-rope-related FD profiles and their evolution (M. Dumbović et al. 2018, 2024). These results suggest that the relative importance of sheath and ejecta in shaping FD profiles is controlled by a combination of shock strength, sheath turbulence, ejecta magnetic field intensity and coherence, and the radial evolution of ICME substructures–conditions that can be substantially modified in interacting CME events.

Analytical and numerical studies further show that CR depression does not occur instantaneously upon encountering enhanced magnetic fields. In the sheath region, the lag between the peak IMF and the CR response has been interpreted as the cross-field diffusion time through the turbulent compressed field (K. P. Arunbabu et al. 2015). In the magnetic ejecta, diffusion-expansion models such as ForbMod (M. Dumbović et al. 2018) show that CRs enter the flux rope via inefficient perpendicular diffusion, and the resulting FD evolves with the flux-rope expansion; the FD minimum within the ejecta thus reflects the time-dependent balance between perpendicular diffusion and expansion, rather than a simple delay relative to the magnetic field peak. The timing of FD onset relative to shock arrival can also vary, with some events showing early decreases due to upstream preconditioning (A. Papaioannou et al. 2020). In interacting CME events, where multiple shocks, sheaths, and compressed ejecta coexist, such timing relationships may become more complex, making it difficult to identify which substructures control the onset, rate, and minimum of the FD.

Upstream preconditioning plays an important role in determining the ability of CMEs to produce FDs. During solar maximum, closely launched CMEs frequently interact as they propagate, forming complex or merged ICMEs and extended interaction regions (IRs) characterized by compressed magnetic fields, enhanced turbulence, and prolonged disturbances (N. Lugaz et al. 2012; M. Temmer et al. 2014; W. Mishra, N. Srivastava & T. Singh 2015a; W. Mishra, Y. Wang & N. Srivastava 2016; W. Mishra et al. 2021). These interacting structures can strengthen diffusion barriers and convective effects over larger spatial scales, producing FDs that differ in amplitude, recovery time, and temporal structure from those associated with isolated CMEs, and are often linked to stronger geomagnetic activity (W. Mishra, N. Srivastava & D. Chakrabarty 2015b; N. S. Shlyk et al. 2022).

Recent studies further suggest that interacting ICMEs are particularly efficient modulators of galactic CRs, often producing larger and more complex FDs than single events (M. Dumbović et al. 2020; A. Papaioannou et al. 2020; N. S. Shlyk et al. 2022). This enhanced modulation is attributed to cumulative effects of multiple shocks, intensified sheaths, and compressed magnetic ejecta formed during CME-CME interactions (J. L. Freiherr von Forstner et al. 2020; E. E. Davies et al. 2023b). For example, D. Maričić et al. (2014) showed that compression of an earlier ICME by a faster trailing CME produced an enhanced magnetic structure associated with a deep and prolonged FD, while N. S. Shlyk et al. (2022) found that the second ICME in interacting pairs can be more effective in modulating CRs than isolated events.

Despite these advances, several key aspects of FD formation in interacting ICME events remain poorly understood. In particular, the relative contributions of individual ICMEs within interacting pairs, along with associated sheath regions and interaction-related structures (W. Mishra et al. 2015a; S. Khuntia, W. Mishra & A. Agarwal 2025), to the rate and depth of CR decrease have not been systematically quantified on an event-by-event basis. Furthermore, the temporal relationships between the peak IMF strength and the FD minimum, and between the FD onset and shock arrival, have not been characterized across multiple interacting events. These timing relationships have implications for space weather forecasting, as they may determine how early CR-based signatures can indicate approaching interplanetary disturbances.

The present study addresses these gaps by analyzing eight well-characterized interacting ICME events observed during solar cycle 24 (2010–2015). For each event, the FD profile is decomposed into contributions from identifiable substructures, and the rate of CR depression (per cent per hour) is quantified separately for the shock-sheath, interacting pairs (ICME1-ICME2), merged ICMEs, and IR. We further examine the time delay between the peak IMF strength and the FD minimum, the relationship between FD onset and shock arrival, and the correspondence between the FD minimum and the geomagnetic Dst minimum. This event-by-event analysis allows us to determine (i) which substructures produce the most rapid CR suppression, (ii) which primarily control the total FD depth, (iii) how the lag between the magnetic field peak and FD minimum varies across different interaction configurations, and (iv) whether early FD onsets in interacting events can serve as precursors of approaching disturbances. The results are presented in Section 3, followed by the conclusions in Section 4.

2 SELECTED EVENTS AND OBSERVATIONS

We examine eight well-documented interacting CME events that occurred during Solar Cycle 24 and were directed towards Earth. These events have been extensively analyzed in previous studies of CME-CME interaction dynamics and are associated with moderate to strong geomagnetic storms. The dates listed below refer to the CME launch times at the Sun as observed in LASCO coronagraph data. The selected events occurred on 2010 May 23–24 (Event 1; N. Lugaz et al. 2012; W. Mishra et al. 2017); 2011 February 13–15 (Event 2; D. Maričić et al. 2014; W. Mishra & N. Srivastava 2014; M. Temmer et al. 2014); 2011 August 3–4 (Event 3; W. Mishra et al. 2017); 2012 January 18–19 (Event 4; Y. D. Liu

Downloaded from academic.oup.com/mnras/article/552/1/stag1664/8785133 by Indian Institute of Astrophysics user on 19 October 2026

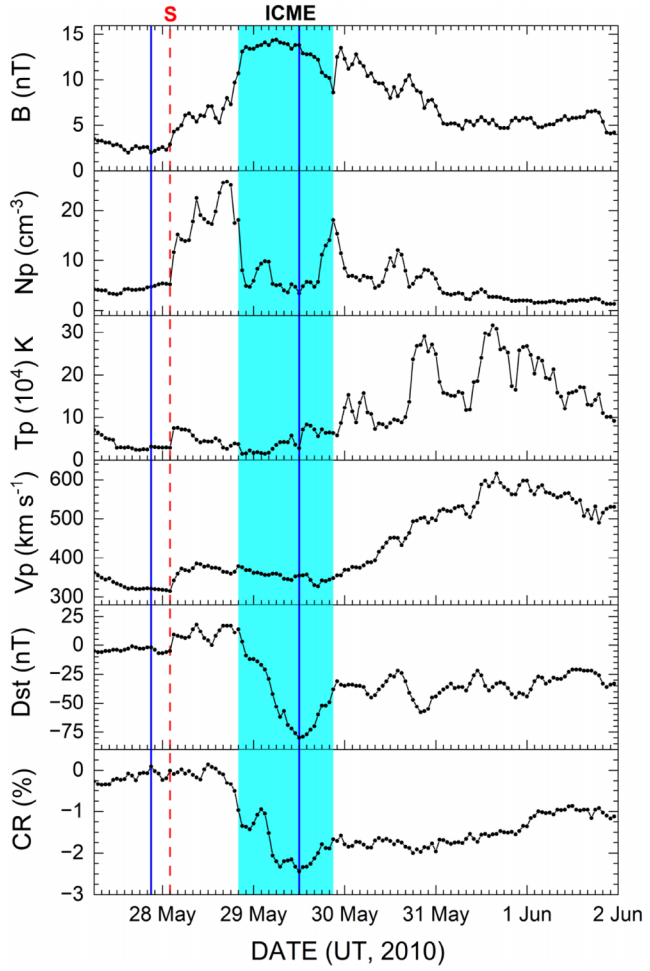


Figure 1. From top to bottom: the total magnetic field strength, proton density, proton temperature, proton speed, Dst index, and CR intensity (on *Y*-axis) for the time interval of May 27 06:00 UT to June 2 00:00 UT, 2010 (on *X*-axis) are shown. From the left, the first and second vertical blue solid lines mark the times of the FD onset and minimum, respectively, while the vertical dashed red line marks the arrival of shock S. The region shaded in cyan represents the interval of the merged ICME.

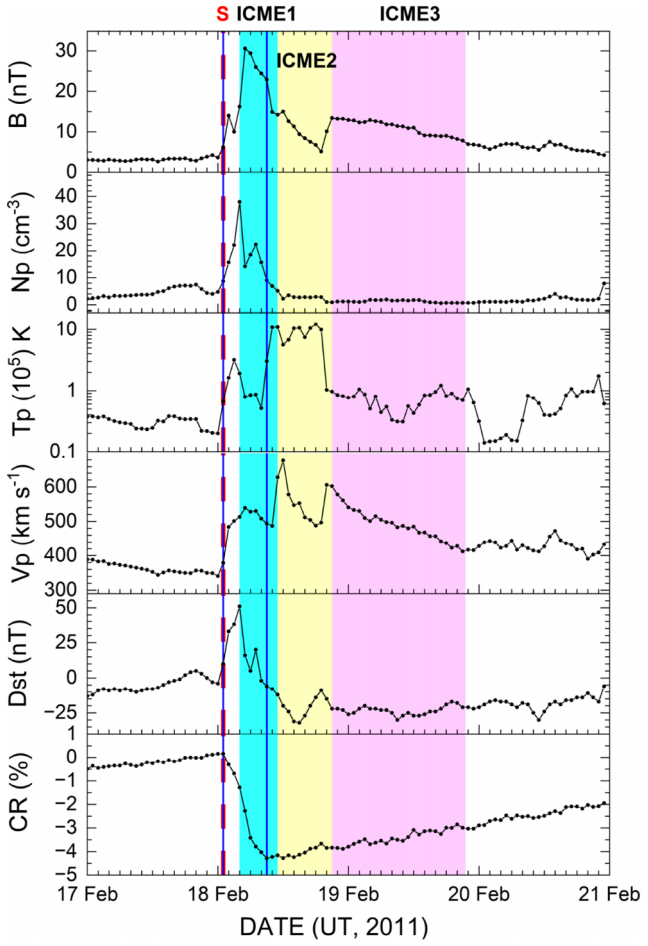


Figure 2. From top to bottom: the total magnetic field strength, proton density, proton temperature, proton speed, Dst index, and CR intensity (on *Y*-axis) for the time interval of February 17 00:00 UT to February 21 00:00 UT, 2011 (on *X*-axis) are shown for Event 2. From the left, the first and second vertical blue solid lines mark the FD onset and minimum times, respectively, and the vertical dashed red line marks the arrival of shock S. The shock and the FD onset time occur simultaneously, and lines representing them overlap. The shaded cyan, yellow, and magenta regions represent the interval of ICME1, ICME2, and ICME3, respectively.

et al. 2013); 2012 June 13–14 (Event 5; W. Mishra et al. 2017; N. Srivastava, W. Mishra & D. Chakrabarty 2018); 2012 September 25–28 (Event 6; W. Mishra et al. 2015a; W. Mishra et al. 2017); 2012 November 9–10 (Event 7; W. Mishra et al. 2015b; W. Mishra et al. 2017); and 2015 March 14–15 (Event 8; Y. D. Liu et al. 2015). The corresponding *in situ* observation intervals at 1 au are shown in Figs 1–8 and Tables 1 and 2.

2.1 Data and methodology

The *in situ* solar wind plasma and magnetic field data were obtained from the OMNI data base[1] (J. H. King & N. E. Papitashvili 2005) with 1-h resolution. The parameters analyzed include the total magnetic field strength (B), proton number density (N_p), proton temperature (T_p), proton bulk speed (V_p), and the Dst geomagnetic index. These parameters are plotted alongside the CR intensity for each event in Figs 1–8 to enable direct visual comparison of the FD profile with the passage of ICME substructures.

The CR data were obtained from the FEID (Forbush Effects and Interplanetary Disturbances) data base, which provides CR intensity parameters derived using the Global Survey Method (GSM; A. Belov et al. 2018) based on measurements from the worldwide neutron monitor network (NMDB[2]) for particles with a rigidity of 10 GV. The FEID data are available at 1-h cadence, which sets the effective temporal resolution for all FD-related measurements in this study. While 1-minute resolution OMNI data are available and would allow more precise identification of substructure boundaries, the hourly CR data that form the basis of our FD analysis limit the meaningful temporal precision to ±1 h for all timing measurements (FD onset, FD minimum, B peak, shock arrival, Dst minimum). Time differences between any two such measurements carry uncertainties of $\pm\sqrt{2} \approx \pm 1.4$ h.

[1] https://cdaweb.gsfc.nasa.gov

[2] http://www01.nmdb.eu/

Downloaded from academic.oup.com/mnras/article/552/1/stag1664/8785133 by Indian Institute of Astrophysics user on 19 October 2026

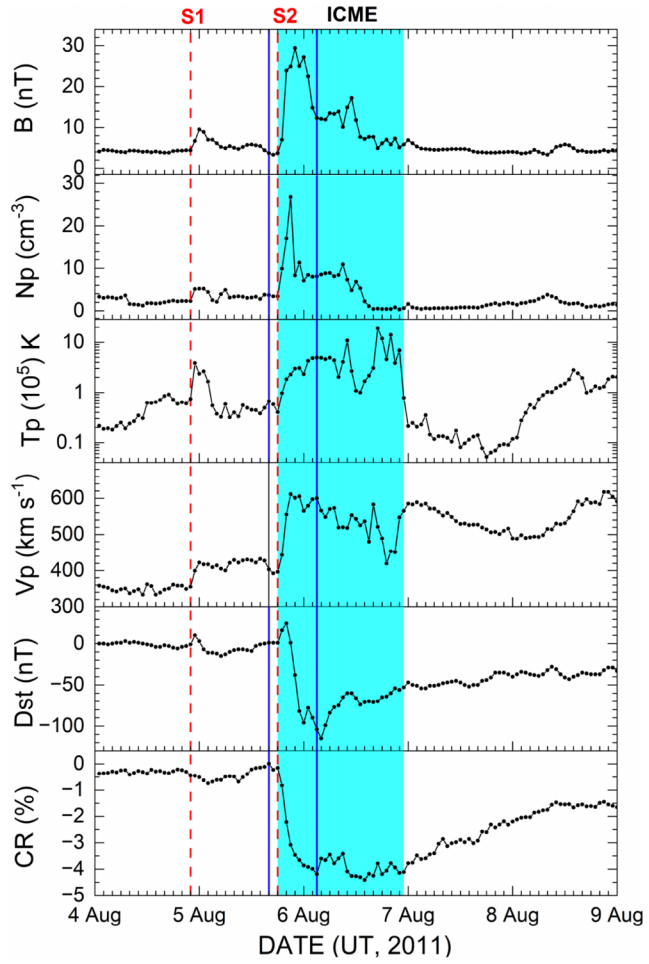


Figure 3. From top to bottom: the total magnetic field strength, proton density, proton temperature, proton speed, Dst index, and CR intensity (on *Y*-axis) for the time interval of August 4 00:00 UT to August 9 00:00 UT, 2011 (on *X*-axis) are shown for Event 3. From the left, the first and second vertical blue solid lines mark the times of the FD onset and minimum, respectively, while the first and second vertical dashed red lines mark the arrivals of shocks S1 and S2. The cyan-shaded region represents the merged ICME interval.

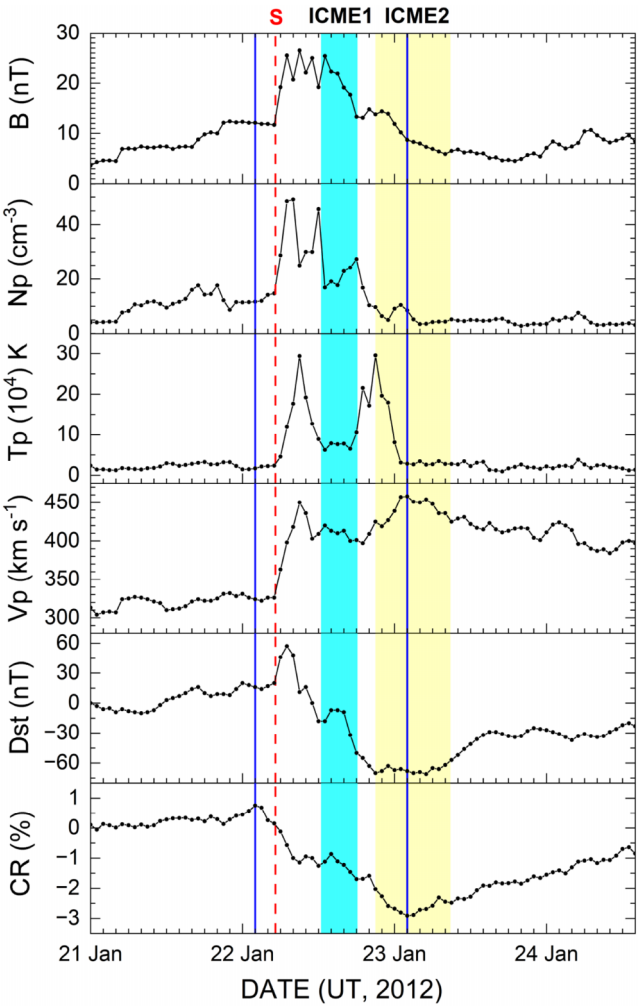


Figure 4. From top to bottom: the total magnetic field strength, proton density, proton temperature, proton speed, Dst index, and CR intensity (on *Y*-axis) for the time interval of 2012 January 21 00:00 UT to January 24 14:00 UT (on *X*-axis) are plotted for Event 4. From the left, the first and second vertical blue solid lines indicate the FD onset and minimum, respectively, and the vertical dashed red line marks the arrival of shock S. The shaded regions represent the interval of ICME1 (cyan colour) and ICME2 (yellow colour).

The identification of ICME substructures, including the interplanetary shock arrival time, the start and end times of the magnetic ejecta, and the classification of the disturbance type, is adopted from the Richardson & Cane near-Earth ICME catalogue[3] (I. G. Richardson & H. V. Cane 2010; I. Richardson & H. Cane 2024). This widely used catalogue provides a systematic identification of ICMEs observed at 1 au based on a comprehensive set of plasma and magnetic field signatures, including enhanced magnetic field strength, smooth field rotation, depressed proton temperature, low plasma beta, declining speed profile, and compositional anomalies where available. By adopting the catalogue boundaries, we ensure that our ICME identifications are consistent with the broader community standards and are not subject to additional subjective bias introduced by our own boundary selection.

For interacting events where two or more ICMEs are observed in close succession, we distinguish between merged' and separate' configurations based on the *in situ* signatures as documented in the published case studies of each event (see references in Section 2). In merged events (Events 1 and 3), the *in situ* data show a single continuous ejecta interval with no clear internal boundary, despite two CMEs having been launched from the Sun; no secondary compression, discontinuity in field rotation, or reset of plasma signatures is observed within the ejecta. In events with separate structures (Events 4, 5, 6, and 7), two distinct ejecta intervals and/or an IR are identifiable. The IR, present in Event 7, is identified as a compressed region between two ejecta that shows elevated magnetic field strength, density, and temperature but does not satisfy the standard magnetic ejecta criteria (no smooth field rotation, no depressed temperature, no low plasma beta).

The FD onset is defined as the hour at which the CR intensity begins a sustained decrease below the pre-event baseline level, where the baseline is defined as the mean CR intensity over the 24 h preceding the event. The FD minimum is the hour of the

[3]https://izw1.caltech.edu/ACE/ASC/DATA/level3/icmetable2.htm

Downloaded from academic.oup.com/mnras/article/552/1/stag1664/8785133 by Indian Institute of Astrophysics user on 19 October 2026

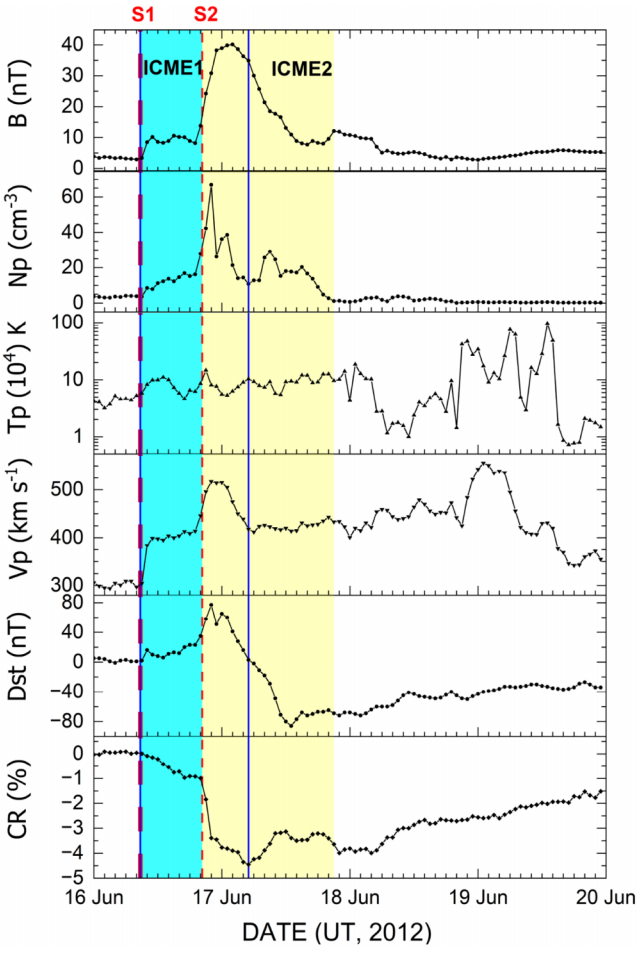


Figure 5. From top to bottom: the total magnetic field strength, proton density, proton temperature, proton speed, Dst index, and CR intensity (on *Y*-axis) for the time interval of 2012 June 16 00:00 UT to June 20 00:00 UT (on *X*-axis) are plotted for Event 5. From the left, the first and second vertical blue solid lines indicate the FD onset and minimum, respectively, while the first and second vertical dashed red lines mark the arrivals of shocks S1 and S2. The shock and the FD onset time occur simultaneously, and lines representing them overlap. The shaded regions in cyan and yellow represent the interval of ICME1 and ICME2, respectively.

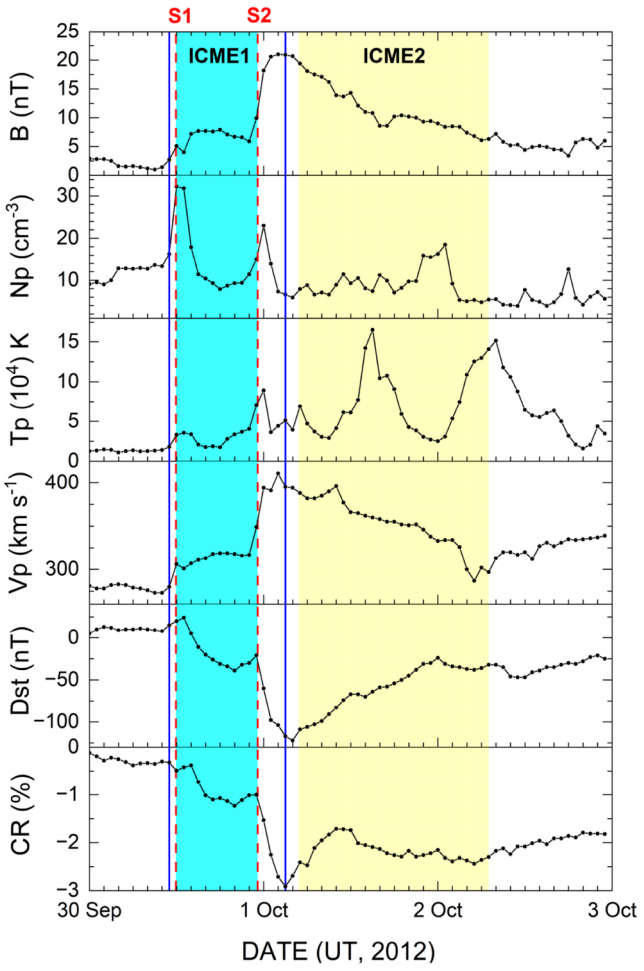


Figure 6. From top to bottom: the total magnetic field strength, proton density, proton temperature, proton speed, Dst index, and CR intensity (on *Y*-axis) for the time interval of 2012 September 30 00:00 UT to October 3 00:00 UT (on *X*-axis) are plotted for Event 6. From the left, the first and second vertical blue solid lines mark the times of the FD onset and minimum, respectively, while the first and second vertical dashed red lines mark the arrivals of shocks S1 and S2. The shaded regions in cyan and yellow represent the interval of ICME1 and ICME2, respectively.

lowest CR intensity during the event. The decline rate within each substructure is calculated as the magnitude of the CR intensity change ($|\Delta$CR$|$ in per cent) divided by the duration (Δt in hours) of that substructure: rate $= |\Delta\text{CR}|/\Delta t$ where the substructure boundaries define Δt and the CR values at the start and end of each interval define ΔCR. The recovery phase is defined as the interval from the FD minimum to the approximate time when the CR intensity returns to within 1σ of the pre-event baseline. We note that the end of recovery is difficult to determine precisely, and recovery durations are reported as approximate values.

We emphasize that with eight interacting events, our sample is insufficient for robust statistical analysis. We therefore present our findings as case-study observations and avoid drawing generalized statistical conclusions. Where possible, we compare our measured values with published ranges for isolated ICME-driven FDs to provide context.

2.2 Event 1: 2010 May 28–June 2

Two CMEs were launched successively from the same active region, NOAA 11072, on 2010 May 23 and 24 with a separation of ∼21 h. The average speeds of the first and second CMEs were ∼370 km s^{-1} and ∼520 km s^{-1}, respectively. The faster second CME caught up with the preceding one, and their interaction was observed at a distance of ∼45 $R_\odot$ from the Sun. After the interaction, the second CME was reported to be deflected, and the merged structure propagated towards Earth as a complex ICME (N. Lugaz et al. 2012; W. Mishra et al. 2017). Fig. 1 shows the variations of the *in situ* plasma and magnetic field parameters together with the CR intensity for this event.

In the context of our focus on interacting CMEs and their associated FDs, the CR intensity begins to decrease in the sheath region, indicating the initial modulation by the disturbed solar wind. A more pronounced decrease occurs within the ICME following the sheath, forming the first step of the FD with a decline rate of ∼0.28 per cent per hour (Fig. 1). A second step is observed within the merged ICME structure, leading to an additional ∼2.5

Downloaded from academic.oup.com/mnras/article/552/1/stag1664/8785133 by Indian Institute of Astrophysics user on 19 October 2026

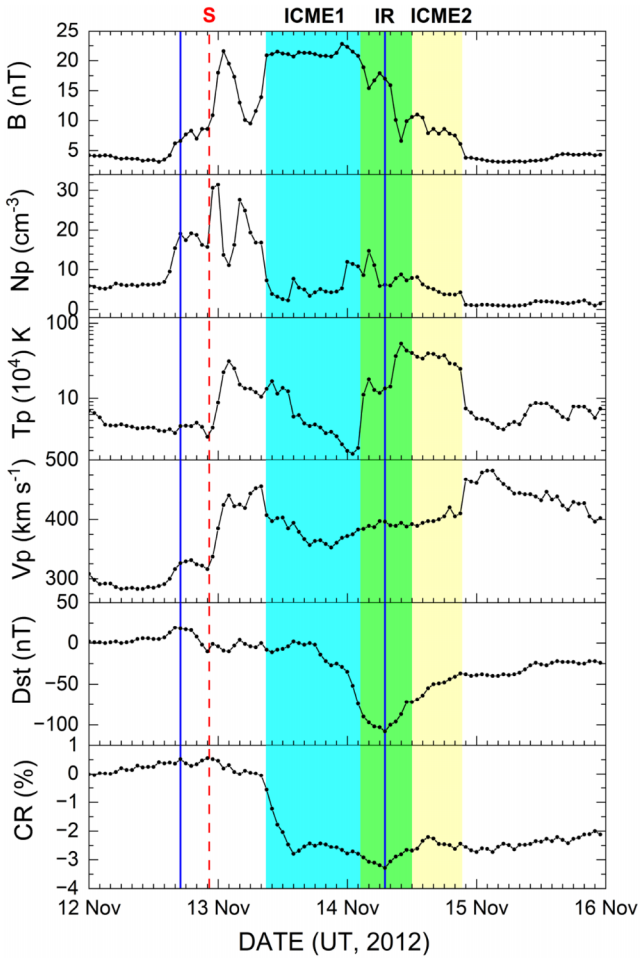


Figure 7. From top to bottom: the total magnetic field strength, proton density, proton temperature, proton speed, Dst index and CR intensity (on *Y*-axis) with time interval of 2012 November 12 00:00 UT to November 16 00:00 UT (on *X*-axis) are plotted for Event 7. From the left, the first and second vertical blue solid lines mark the times of the FD onset and minimum, respectively, and the vertical dashed red line marks the arrival of shock S. The shaded regions in cyan, green, and yellow represent the interval of ICME1, IR, and ICME2, respectively.

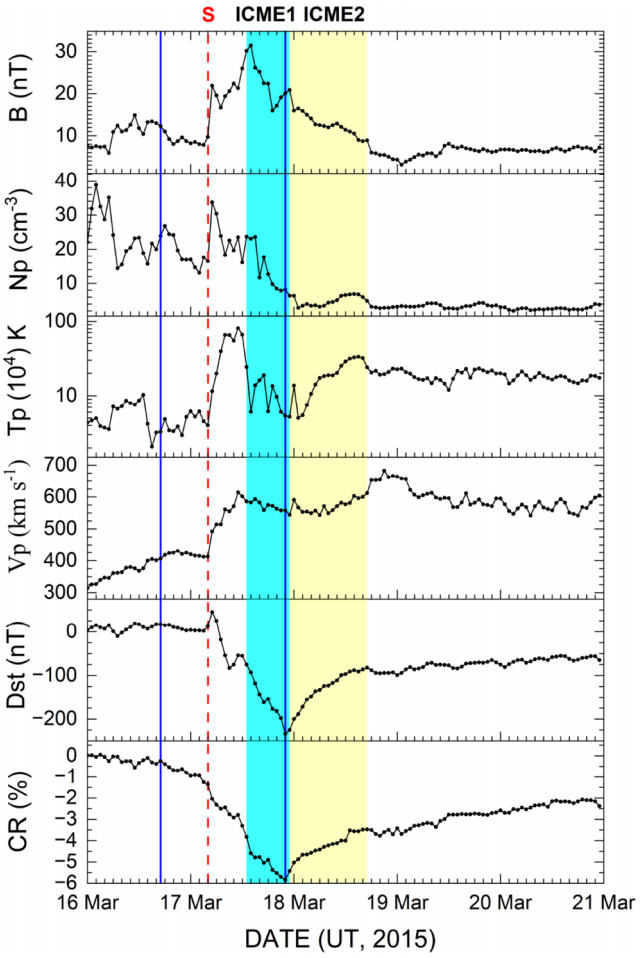


Figure 8. From top to bottom: the total magnetic field strength, proton density, proton temperature, proton speed, Dst index, and CR intensity (on *Y*-axis) with time interval of 2015 March 16 00:00 UT to March 21 00:00 UT (on *X*-axis) are plotted for Event 8. From the left, the first and second vertical blue solid lines indicate the FD onset and minimum, respectively, and the vertical dashed red line marks the arrival of shock S. The shaded regions in cyan and yellow represent the interval of ICME1 and ICME2, respectively.

per cent decrease with a slower decline rate of ∼0.14 per cent per hour. These features indicate that the dominant contribution to the FD arises from the interacting ICME structure rather than the sheath alone. The recovery phase lasts for more than 3 d.

The peak magnetic field strength within the ICME reaches 14.4 nT, occurring about 6 h prior to the minimum CR intensity. The maximum FD is observed at 12:00 UT on May 29, coinciding with the minimum Dst (∼−80 nT) and showing no significant time delay, suggesting a close association among the interacting ICME structure, geomagnetic activity, and the observed FD.

During the ICME interval, the Dst index decreases smoothly and reaches its minimum near the middle of the ICME, then gradually recovers towards the trailing edge. The CR intensity also shows a gradual decrease throughout the ICME, with a minimum near the Dst minimum. During the CR decreasing phase, the drop begins near the ICME leading region and continues into the central ICME, coinciding with enhanced magnetic field. The onset of the decrease follows a density enhancement, suggesting a possible density effect. However, the CR continues to decrease as density declines, while speed and temperature are showing no clear correspondence with the CR profile.

2.3 Event 2: 2011 February 17−21

Three Earth-directed CMEs were launched successively from the same active region, NOAA 11158, during 2011 February 13−15 (D. Maričić et al. 2014; W. Mishra & N. Srivastava 2014; M. Temmer et al. 2014; W. Mishra et al. 2017). The first CME (CME1) was observed at 18:36 UT on February 13 as a partial halo CME, the second CME (CME2) at 18:24 UT on February 14 as a halo CME, and the third CME (CME3) at 02:05 UT on February 15 as a halo CME in the field of view of the C2 coronagraph onboard SOHO/LASCO (G. E. Brueckner et al. 1995). The interaction between CME2 and CME3 was observed at a distance of ∼ 24–28 $R_\odot$, while CME1 and CME2 interacted farther out at ∼ 138–157 $R_\odot$ from the Sun (W. Mishra & N. Srivastava 2014). These successive eruptions and their subsequent interactions resulted in a complex ICME structure propagating towards Earth.

Downloaded from academic.oup.com/mnras/article/552/1/stag1664/8785133 by Indian Institute of Astrophysics user on 19 October 2026

Table 1. Interacting CME events: Dst minimum, FD peak, IMF peak, and time offsets between Dst and FD peaks, B and FD peaks, and FD onset relative to shock arrival.

Date	Dst peak (nT)	FD peak (per cent)	Δt(Dst peak-FD peak) (h)	Peak B (nT)	Δt(FD peak-B peak) (h)	Δt(shock arrival-FD onset) (h)
2010 May 28–June 2	−80	−2.44	0	14.4	6	5
2011 February 17–21	−32	−4.29	6	30.6	4	0
2011 August 5–9	−115	−4.2	1	29.4	5	2
2012 January 21–24	−71	−2.91	3	26.5	17	3
2012 June 16–18	−86	−4.45	8	40.1	3	0
2012 September 30–October 3	−122	−2.91	1	21	1	1
2012 November 12–16	−108	−3.28	0	22.8	8	5
2015 March 16–21	−223	−5.84	0	31.5	8	11

Table 2. Interacting CME events: FD amplitudes and decline rates within each identifiable ICME substructure, and the substructure with the largest ΔCR.

Date of ICME	Dst peak (nT)	FD amplitude (per cent)	Rate of FD (% h^{-1})	Largest ΔCR substructure
2010 May 28–June 2	−80	1.11 (sheath)	0.14 (sheath)	Merged ICME
		1.38 (merged ICME)	0.28 (merged ICME)	
2011 February 17–21	−32	1.44 (ICME1 sheath)	0.48 (ICME1 sheath)	ICME1
		4.45 (ICME1)	0.60 (ICME1)	
2011 August 5–9	−115	4.05 (merged ICME)	0.45 (merged ICME)	Merged ICME
2012 January 21–24	−71	0.40 (ICME1 sheath)	0.06 (ICME1 sheath)	ICME2
		0.83 (ICME1)	0.20 (ICME1)	
		1.32 (ICME2)	0.22 (ICME2)	
2012 June 16–18	−86	0.98 (ICME1)	0.08 (ICME1)	ICME2
		3.46 (S2 + ICME2)	0.68 (S2 + ICME)	
2012 September 30–October 3	−122	0.85 (ICME1)	0.21 (ICME1)	ICME2
		1.91 (ICME2)	0.21 (ICME2)	
2012 November 12–16	−108	1.11 (sheath)	0.10 (sheath)	IR
		2.23 (ICME1)	0.45 (ICME1)	
		0.49 (IR)	0.10 (IR)	
2015 March 16–21	−223	2.47 (ICME1 sheath)	0.28 (ICME1 sheath)	ICME1
		2.02 (ICME1)	0.25 (ICME1)	

Fig.2 shows the variations of *in situ* plasma and magnetic field parameters together with the CR intensity for this event. In the context of interacting CMEs and their associated FDs, the CR intensity begins to decrease with the arrival of the IP shock. The decrease continues through the sheath and into the ICME1 region, reaching a maximum reduction of ≈4.3 per cent. The decline rate is ∼0.48 per cent per hour in the ICME1 sheath and increases to ∼0.6 per cent per hour within ICME1, indicating that the dominant contribution to the FD arises from the first ICME associated with the interacting CME system. The recovery phase of the FD is unusually long, lasting more than 3 d.

The minimum CR intensity occurs at 09:00 UT on 2011 February 18 approximately 6 h before the minimum Dst value (∼−32 nT). The peak magnetic field strength reaches ∼31 nT within the ICME1 region, occurring about 4 h prior to the minimum CR intensity. These features suggest that the interacting CME-driven ICME structure, particularly ICME1, plays the primary role in producing the observed FD. It is worth noting that while the FD magnitude is primarily determined by magnetic field strength, turbulence, and diffusion barriers within the interacting ICME, the Dst response depends primarily on the duration and magnitude of the southward IMF component.

It is important to note that this event produced only a weak geomagnetic storm with a minimum Dst of ∼−32 nT. Consequently, despite a clear FD associated with the interacting CMEs, the relatively weak geomagnetic response results in a poor correspondence between FD and Dst timing for this event. This behavior contrasts with the other selected events, in which stronger geomagnetic activity allows a more direct and meaningful comparison between the FD and Dst minima.

During the sequence of three ICMEs, the Dst index shows a stepwise decrease, with an initial disturbance near ICME1, a deeper minimum during ICME2, and then a gradual recovery through ICME3. The CR intensity exhibits a sharp Forbush decrease starting at ICME1, reaches its minimum towards the rear edge of ICME1, and then slowly recovers across ICME2 and ICME3. The onset of the decreases coincides with increases in solar wind density, speed, and temperature, suggesting that these parameters may play a secondary role at the onset. CR variations seem to be primarily governed by the intervals of enhanced magnetic field, and do not closely follow the density, temperature, or speed variations.

2.4 Event 3: 2011 August 5–9

Two CMEs were launched successively from the same active region, NOAA 11261, on 2011 August 3 and 4 with a separation of ∼14 h. The first CME (CME1), with a speed of ∼610 km s^{-1}, was observed at 14:00 UT on August 3, while the second CME (CME2), with a higher speed of ∼1315 km s^{-1}, was observed at

Downloaded from academic.oup.com/mnras/article/552/1/stag1664/8785133 by Indian Institute of Astrophysics user on 19 October 2026

04:12 UT on August 4. Both CMEs appeared as halo events in the field of view of the LASCO-C2 coronagraph onboard SOHO. The faster CME2 caught up with CME1, and their interaction was inferred at a distance of ∼145 $R_\odot$ from the Sun. The interacting CMEs subsequently merged into a single ICME and propagated towards Earth (W. Mishra et al. 2017). Fig. 3 shows the variations of *in situ* plasma and magnetic field parameters together with the CR intensity for this event.

In the context of interacting CMEs and their associated FDs, the CR intensity decreases sharply with the arrival of the IP shock, indicating the onset of CR modulation by the disturbed solar wind. The decrease continues through the sheath and reaches its maximum amplitude of ≈4.2 per cent within the merged ICME region. The decline rate of the FD is ∼0.45 per cent per hour, suggesting that the dominant contribution to the FD arises from the interacting ICME structure. The recovery phase of the FD lasts for more than 2 d.

The minimum CR intensity occurs at 03:00 UT on 2011 August 6 coinciding with the passage of the ICME at Earth. The peak magnetic field strength within the ICME reaches ∼30 nT, occurring about 5 h prior to the FD minimum. The FD minimum at 03:00 UT on August 6 coincides with the minimum Dst value of ∼−115 nT, with no significant time delay between them. This close correspondence between the FD and Dst minima indicates that the interacting CME-driven merged ICME structure is responsible for both the enhanced geomagnetic activity and the observed FD.

During the merged ICME interval, the Dst index decreases sharply after S2 and reaches its minimum within the early part of the ICME, followed by a gradual recovery towards the trailing edge. The CR intensity also shows a rapid decrease beginning near S2, with the minimum occurring within the merged ICME, and recovery thereafter.CR decreases occur during the interval of an enhanced magnetic field. During the CR decrease phase, it appears that enhanced density, speed, and temperature in the ICME leading region may contribute to the initial and early decrease, but they do not exert consistent control over the entire CR depression.

2.5 Event 4: 2012 January 21−24

Two CMEs were launched successively from the active regions NOAA 11 401 and 11 402 during 2012 January 18–19. The first CME (CME1) was observed at 13:25 UT on January 18 as a partial halo CME, followed by the second CME (CME2) at 15:10 UT on January 19 as a halo CME. The interaction between the two CMEs was reported to occur at a distance of ∼85 $R_\odot$ from the Sun, and the structures subsequently propagated towards Earth, where they were identified as distinct but closely spaced ICMEs (Y. D. Liu et al. 2013). Fig. 4 shows the variations of the *in situ* plasma and magnetic field parameters together with the CR intensity for this event.

For this event, we note that the CR intensity begins to decrease about 3 h prior to the arrival of the interplanetary shock. The sheath region corresponds to the first step of the FD, producing a decrease of ∼1.2 per cent. The passage of ICME1 leads to a further decrease of ∼1.7 per cent. The second, more gradual decrease is associated with ICME2, during which the CR intensity reaches a minimum of ∼3 per cent at 02:00 UT on 2012 January 23. The recovery phase begins near the trailing edge of the ICME structure and lasts for more than 2 d. These features indicate that both ICMEs contribute to the FD, with ICME2 providing the dominant decrease.

The decline rate of the FD is ∼0.06 per cent per hour in the ICME1 sheath, ∼0.20 per cent per hour within ICME1, and ∼0.22 per cent per hour within ICME2. The FD minimum occurs at 02:00 UT on January 23, followed by the minimum Dst value (∼−71 nT) approximately 3 h later. The peak magnetic field strength reaches 26.5 nT, occurring about 17 h prior to the FD minimum and approximately 3 h after the onset of the FD (A. Papaioannou et al. 2020). These observations suggest that the interacting CME-driven structures produce a multistep FD, with ICME2 acting as the primary contributor to the overall FD amplitude.

During the successive ICME intervals, the Dst index begins to decrease after the shock-driven SSC and then Dst reaches its minimum during ICME2, followed by a gradual recovery afterward. The CR intensity also starts decreasing after the shock, continues to decline through ICME1, and reaches its minimum within ICME2, before gradually recovering. The CR decrease occurs during the period of enhanced magnetic field, while the density shows a brief enhancement near the shock and within ICME1 that does not persist throughout the CR depression. During the initial phase of the CR decrease, increases in solar wind speed and temperature near the shock and ICME1 appear to coincide with the onset and early drop in CR intensity; however, these parameters do not show a consistent correspondence with the entire CR decrease, which continues into ICME2.

2.6 Event 5: 2012 June 13–14

Two CMEs originating from the same active region, NOAA 11504, were launched on 2012 June 13 and 14 separated by several hours. The first and second CMEs had average speeds of ∼630 and ∼990 km s^{-1}, respectively. The faster second CME caught up with the preceding one, and the interacting structures propagated towards Earth as a merged ICME (W. Mishra et al. 2017; N. Srivastava et al. 2018). Fig. 5 shows the variations of *in situ* plasma and magnetic field parameters together with the CR intensity for this event.

The interplanetary structure is bounded by two shocks, S1 and S2. The region between S1 and S2 corresponds to ICME1, lasting for ∼11 h. During the passage of ICME1, the magnetic field strength reaches ≈10 nT, while the CR intensity shows only a gradual decrease of about 1 per cent, indicating a relatively weak modulation by the first ICME. A more pronounced decrease in CR intensity begins with the arrival of the second shock (S2), marking the entry into the stronger, interacting ICME. Following S2, the magnetic field increases sharply to ≈40 nT, and the CR intensity decreases further, reaching ∼3.5 per cent about 3 h later.

The CR intensity continues to decline within the merged ICME structure, attaining a minimum value of ∼4.45 per cent at 05:00 UT on June 17. This minimum is followed by the minimum Dst value (∼−86 nT) approximately 8 h later. The recovery phase of the FD is prolonged, lasting for more than 4 d. The FD onset closely corresponds to the arrival of shocks S1 and S2, indicating that both shocks and the subsequent ICME structures contribute to the observed modulation.

Both ICME1 and ICME2 contribute to the multistep FD, although their relative roles differ. The decline rate of the FD is ∼0.08 per cent per hour within ICME1, while a rapid decrease of ∼1.2 per cent per hour is observed near the shock-associated SSC. Within the merged ICME2 structure, the decline rate is ∼0.15

Downloaded from academic.oup.com/mnras/article/552/1/stag1664/8785133 by Indian Institute of Astrophysics user on 19 October 2026

per cent per hour, indicating that ICME2 provides the dominant contribution to the overall FD amplitude. The absence of a well-defined sheath region and the stronger magnetic field within ICME2 suggest that the interacting and merged ICME structure is primarily responsible for the observed FD.

During the CR decreasing phase, the intensity begins to drop within ICME1 and declines more rapidly after S2, reaching its minimum in the early part of ICME2. This decrease coincides with the interval of enhanced magnetic field spanning late ICME1 and early ICME2. The initial decrease in CR coincides with enhanced magnetic field, along with increased density and speed near S2, suggesting a possible contribution during the early phase. However, the CR continues to decrease with no clear dependence on speed and density.

2.7 Event 6: 2012 September 30–October 3

Two CMEs were launched successively from the same active region, NOAA 11575, during 2012 September 25–28. The first CME (CME1) occurred at 11:24 UT on September 25 with a speed of ∼335 km s^{-1}, while the second CME (CME2) was observed at 00:12 UT on September 28 as a full halo CME with a speed of ∼950 km s^{-1}. W. Mishra et al. (2015a, 2017) reported that the interaction between the two CMEs occurred close to Earth at a distance of ∼215 $R_{\odot}$ and beyond. Following the interaction, the structures propagated towards Earth and were identified as separate but closely spaced ICMEs (W. Mishra et al. 2015a). Fig. 6 shows the variations of *in situ* plasma and magnetic field parameters together with the CR intensity for this event.

The interplanetary structure is bounded by two shocks, S1 and S2, with ICME1 located in the region between them and lasting for ∼11 h. During the passage of ICME1, the magnetic field strength reaches ≈6 nT, while the CR intensity decreases gradually by ∼1.2 per cent, corresponding to a decline rate of ∼0.21 per cent per hour. A more pronounced decrease in CR intensity begins with the arrival of shock S2, marking the entry into the second ICME structure. Following S2, the magnetic field increases to ≈22 nT, and the CR intensity decreases further, reaching ∼3 per cent about one hour later.

The FD reaches its maximum amplitude at 03:00 UT on October 1 within ICME2. This minimum in CR intensity is followed by the minimum Dst value (∼−122 nT) approximately 1 h later, indicating a close temporal correspondence between the FD and geomagnetic response. The recovery phase of the FD lasts for more than 2 d. The onset of the CR decrease coincides well with the arrivals of shocks S1 and S2, suggesting that both shocks and the subsequent ICME structures contribute to the observed modulation.

Both ICME1 and ICME2 contribute to the multistep FD, although their relative contributions differ. The gradual decrease associated with ICME1 is followed by a stronger modulation within ICME2, indicating that ICME2 acts as the primary contributor to the overall FD amplitude. No well-defined sheath region is identified for this event, and the stronger magnetic field within ICME2 supports its dominant role in producing the observed FD.

During the ICME interval, the Dst index begins to decrease after the S1-driven rise and drops more sharply following the S2-driven rise, reaching its minimum near the ICME1-ICME2 transition, then gradually recovering through ICME2. The CR intensity also starts decreasing within ICME1, shows a sharper drop after S2, and reaches its minimum near the beginning of ICME2 before gradually recovering afterward. The CR decrease occurs during the interval of enhanced magnetic field spanning late ICME1 and early ICME2. The increases in solar wind density, speed, and temperature around S2 and near the ICME1-ICME2 transition appear to coincide with the onset and early reduction in CR intensity; however, these parameters do not show a consistent correspondence with the entire CR depression, which extends into ICME2.

2.8 Event 7: 2012 November 12–16

Two CMEs were launched a few hours apart on 2012 November 9 and 10 from active region NOAA 11608, with speeds of ∼620 and ∼910 km s^{-1}, respectively. The CMEs propagated in nearly the same direction, and their interaction was observed at a distance of ∼35 $R_{\odot}$ from the Sun. Following the interaction, the combined structure propagated towards Earth as a merged ICME (W. Mishra et al. 2015b; W. Mishra et al. 2017). Fig. 7 shows the variations of the *in situ* plasma and magnetic field parameters together with the CR intensity for this event.

In the context of our study, the CR intensity begins to decrease with the arrival of the IP shock. The initial decrease occurs within the sheath region, producing a modest reduction of ∼0.5 per cent with a decline rate of ∼0.1 per cent per hour. A more pronounced second step of the FD is observed within ICME1, where the CR intensity decreases to ∼3 per cent with a decline rate of ∼0.45 per cent per hour. The decrease continues within the IR, leading to a maximum FD amplitude of ∼3.5 per cent with a slower decline rate of ∼0.1 per cent per hour. These features indicate that both ICME1 and the IR contribute to the multistep FD, with the IR providing the dominant contribution to the overall FD amplitude.

The peak magnetic field strength reaches ∼23 nT within ICME1, occurring about 8 h prior to the FD minimum. The maximum FD is observed at 07:00 UT on November 14, coinciding with the minimum Dst value (∼−108 nT) with no significant time delay. The recovery phase of the FD is prolonged, lasting for more than 2 d. This close correspondence between the FD and Dst minima suggests that the interacting CME-driven merged ICME and the associated IR play a key role in producing both the geomagnetic response and the observed FD.

We note that the Dst index shows a gradual decrease after the S-driven rise, with a stronger decline through ICME1 and reaching its minimum within the IR, followed by recovery during ICME2. The CR intensity also begins to decrease within ICME1, continues declining through the IR, and attains its minimum near the IR-ICME2 transition before gradually recovering. The CR decrease occurs during the interval of enhanced magnetic field spanning ICME1 and the IR. The increases in solar wind speed, temperature, and density near the shock and early ICME1 appear to contribute to the onset and early drop in CR intensity; however, these parameters do not consistently control the overall CR depression.

2.9 Event 8: 2015 March 16−21

Two CMEs were launched successively from the same active region, NOAA 12297, on 2015 March 14 and 15 separated by ∼16 h. The average speeds of the first and second CMEs were ∼350 and ∼1120 km s^{-1}, respectively. The faster second CME rapidly caught up with the preceding slower CME, and their interaction was reported to occur close to the Sun (Y. D. Liu et al. 2015).

Downloaded from academic.oup.com/mnras/article/552/1/stag1664/8785133 by Indian Institute of Astrophysics user on 19 October 2026

The early interaction led to the formation of a compressed and complex ICME structure that subsequently propagated towards Earth. Fig. 8 shows the variations of the *in situ* plasma and magnetic field parameters together with the CR intensity for this event.

We note that the CR intensity begins to decrease about 11 h prior to the arrival of the IP shock, indicating modulation by the approaching disturbed solar wind and enhanced turbulence ahead of the shock. A pronounced first decrease occurs within the sheath region, where the FD reaches ∼4 per cent at 13:00 UT on 2015 March 17 with a decline rate of ∼0.28 per cent per hour. A further decrease is observed within ICME1, with a decline rate of ∼0.25 per cent per hour, suggesting continued CR modulation by the enhanced magnetic field and diffusion barrier within the interacting ICME. These features indicate that both the sheath and ICME contribute to the FD, with ICME1 providing the dominant contribution to the overall amplitude.

The magnetic field strength reaches a peak value of ∼32 nT within ICME1, occurring about 8 h prior to the FD minimum. The FD attains its maximum amplitude at 22:00 UT on March 17, which coincides with the minimum Dst value (∼−223 nT) with no observable time delay. An earlier decrease in Dst to ∼−100 nT is associated with the sheath region, whereas the main geomagnetic storm development corresponds to the ICME passage. The near-simultaneous occurrence of the FD and Dst minima suggests that the same large-scale magnetic structure is responsible for both cosmic-ray modulation and ring current enhancement. The strong and compressed magnetic field within the ICME provides an efficient diffusion barrier for CR while simultaneously facilitating enhanced geomagnetic activity. The recovery phase of the FD is prolonged, lasting for more than 3 d, consistent with the extended spatial scale and complex magnetic structure of the ICME.

From the figure, we note that the Dst index begins to decrease after the S-driven rise and drops rapidly through ICME1, reaching its minimum near the end of ICME1, followed by a gradual recovery during ICME2. The CR intensity also shows a sharp decrease after the shock, continues to decline throughout ICME1, and attains its minimum near the rear edge of ICME1 before gradually recovering afterward. The CR decrease occurs during the interval of the enhanced magnetic field associated with ICME1. During the initial phase of the CR decrease, elevated solar wind density near the shock and early ICME1, together with increased speed and temperature, appear to contribute to the onset and rapid drop in CR intensity; however, these parameters do not consistently follow the entire CR depression, which continues until the end of ICME1.

3 RESULTS AND DISCUSSION

All eight interacting ICME events analyzed in this study produced clear non-recurrent (ICME-driven) FDs observed in the FEID CR intensity data at a rigidity of 10 GV. The FD amplitudes range from approximately 2.5 per cent to 5.8 per cent, with the largest depression corresponding to the most intense geomagnetic storm (Dst ≈ −223 nT) on 18 March 2015 (Table 1). For comparison, I. G. Richardson & H. V. Cane (2011) reported median FD amplitudes of ∼2–3 per cent for isolated ICMEs at neutron monitor rigidities, and M. Janvier et al. (2021) found average values of ∼2–4 per cent using superposed epoch analysis. The amplitudes observed in our interacting events (six of eight exceeding 2.9 per cent) are within or above this range, though

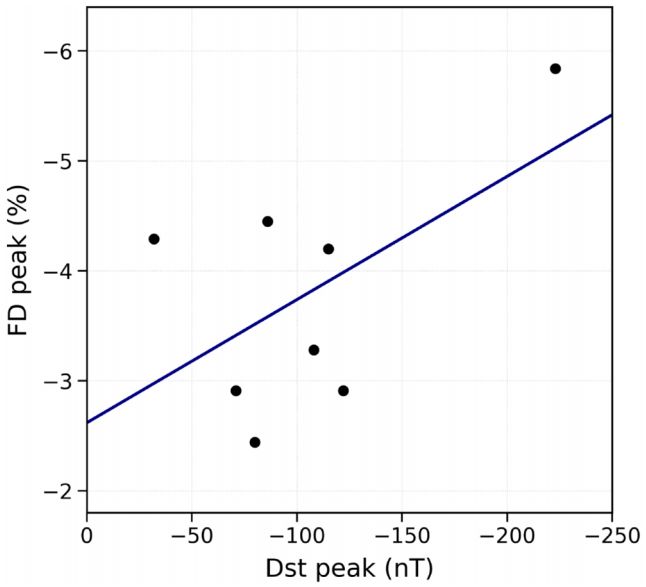


Figure 9. Correlation between Dst peak and FD peak for eight interacting events analysed. The solid line shows the best linear fit, and the inset gives the Pearson and Spearman correlation coefficients.

our sample is too small to establish whether interacting events systematically produce larger FDs. Fig. 9 shows only a moderate correlation between the FD peak and the Dst peak, and the noticeable scatter indicates that FD amplitude and geomagnetic activity are governed by different physical processes.

In most cases, the FD profile exhibits a multistep structure, with two or more distinct decrease phases corresponding to successive ICME substructures such as sheath regions, ICME1/ICME2 regions, merged ICME regions, or IRs. This behavior is clearly visible in Figs 1–8, where step-like decreases in CR intensity correspond to enhancements in solar wind speed, plasma density, and IMF strength. These multistep profiles reflect the sequential passage of multiple modulating substructures, a feature that distinguishes interacting events from isolated ICMEs, which typically produce simpler single-step or two-step (sheath + ejecta) decreases (H. V. Cane 2000; M. Janvier et al. 2021).

A genuine, three-step FD profile (sheath followed by two sequential ejecta/IR steps) is identified in two of the eight events (Events 4 and 7; Table 2), a configuration that is not possible for an isolated ICME, which by definition contains at most one ejecta and hence at most a two-step FD. In four further events (1, 3, 5, and 6), the FD is built from two ejecta-related steps with a weak or absent sheath contribution. For example, no sheath signature was identified in Events 5 and 6, so that both decrease steps originate from ejecta material rather than the classical sheath-then-ejecta sequence. This ejecta-ejecta or ejecta-IR-ejecta sequencing is, to our knowledge, not reported for isolated ICME events and represents a genuine structural difference introduced by the CME-CME interaction. By contrast, the quantitative properties of the FDs, namely the amplitude range (2.5–5.8 per cent), the per-substructure decline rates (0.06–1.2 per cent h^{-1}), and the recovery durations (2–4 d), fall within the ranges reported for isolated ICME-driven FDs (I. G. Richardson & H. V. Cane 2011; M. Janvier et al. 2021). We therefore find that the interacting events analyzed here are distinguished from isolated ICMEs primarily by the number and sequencing of modulating substructures, rather

Downloaded from academic.oup.com/mnras/article/552/1/stag1664/8785133 by Indian Institute of Astrophysics user on 19 October 2026

than by a systematic enhancement of the physical parameters within any individual substructure.

The timing of FD onset relative to the arrival of IP shocks shows significant variability across different events. In four out of eight cases (Events 2, 3, 5, and 6), the onset of the FD coincides closely with the shock arrival time within the ±1.4 h measurement uncertainty), indicating modulation associated with the sheath region. However, in the remaining four events, the onset of FD occurs before the arrival of the shock by 3–11 h (Events 1, 4, 7, and 8). For Events 7 and 8, the offsets of 5 and 11 h substantially exceed the measurement uncertainty and indicate genuine early onsets. Early FD onsets prior to shock arrival suggest that CR modulation can begin upstream of the shock, likely due to enhanced turbulence and magnetic field compression in that region, or to the presence of preceding ICME material. Similar early onsets have been reported by A. Papaioannou et al. (2020), who classified FD events based on the time delay between IMF enhancement and FD profile (the t_H parameter). We note that early onsets are also occasionally reported for isolated ICMEs, but the presence of preceding CME material in interacting events may make them more likely in such configurations.

Table 2 shows that the substructure with the largest CR intensity decrease (ΔCR) varies between events: ICME1 in two cases, ICME2 in three, merged ICME in two, and the IR in one. We note that identifying the substructure with the largest ΔCR does not necessarily identify the 'main driver' of the FD, since in isolated events the sheath and ejecta can contribute comparably even when the FD minimum falls within the ejecta (I. G. Richardson & H. V. Cane 2011). The peak IMF strength associated with FD minima ranges from ∼14 to 40 nT (Table 1). Events with higher peak B tend to show larger FD amplitudes, consistent with M. Janvier et al. (2021), though our sample of eight events is insufficient to establish an independent correlation.

A lag is observed between the time of maximum IMF strength (B) and the FD minimum, ranging from 1 to 17 h (±1.4 h uncertainty) across all events (Table 1). The physical origin of this lag depends on the substructure in which the B peak occurs. For events where the B peak is in the sheath region, the lag can be interpreted as the cross-field diffusion time of CRs into the region of enhanced turbulent magnetic field (K. P. Arunbabu et al. 2015). For events where the B peak occurs within the magnetic ejecta, the FD minimum reflects the time-dependent balance between perpendicular diffusion into the expanding flux rope and its expansion, as described by diffusion-expansion models (M. Dumbović et al. 2018). In this case the lag is not simply a spatial diffusion delay but reflects the evolving ejecta structure. The longest lag (∼17 h) is observed in the January 2012 event, where multiple ICME substructures contribute sequentially. In such cases, the measured lag between the global B peak and the global FD minimum may additionally reflect the cumulative passage of successive modulating regions, which cannot be disentangled with the present data.

The rate of decline in CR intensity varies between different ICME substructures (Table 2). In several events, the ejecta or merged ICME regions exhibit decline rates comparable to or exceeding those of the sheath (e.g. Event 2: 0.60 per cent h^{-1} in ICME1 versus 0.48 per cent h^{-1} in sheath; Event 3: 0.45 per cent h^{-1} in merged ICME). The fastest rate (1.2 per cent h^{-1} in Event 5) is associated with the second shock arrival rather than a classical sheath. These observations suggest that in interacting events, the compressed ejecta can produce rapid CR decreases, likely because compression during CME–CME interaction amplifies the magnetic field within the ejecta beyond typical isolated-ICME values. We therefore do not find a systematic pattern in which the sheath always produces faster decreases than the ejecta; rather, the relative rates vary between events depending on the magnetic field strength and compression within each substructure.

The time delay between the minimum FD and the minimum Dst index ranges from 0 to 8 h. In three events, the FD minimum coincides with the Dst minimum, while in others the geomagnetic response lags behind the CR modulation. This behavior is consistent with earlier findings that FD and geomagnetic storms are related but not causally identical phenomena (R. P. Kane 2010; B. Badruddin et al. 2019). The observed delays suggest that, while both FD and Dst are driven by the same interplanetary structures, they respond to different physical parameters: CRs are primarily sensitive to magnetic field strength and turbulence, whereas geomagnetic activity depends strongly on the southward IMF component and the solar wind electric field. The close correspondence observed in several interacting events indicates that strongly compressed magnetic structures can simultaneously influence CR modulation and geomagnetic activity.

All interacting ICME events analyzed in this study exhibit recovery phases lasting between 2 and 4 d, with Events 5 and 8 extending beyond 4 d. For comparison, H. V. Cane (2000) reported that for isolated ICME-driven FDs the recovery duration typically ranges from 3 to 10 d, with an average of approximately 5 d. Our observed recovery durations of 2–4 d therefore fall within the lower end of the range reported for isolated ICMEs, and we do not claim they are systematically prolonged. The recovery phase of FDs extends well beyond the passage of the ICME structures at 1 au, as the ambient CR density is gradually re-established through diffusion from the surrounding heliosphere after the disturbed region has passed (H. V. Cane 2000; M. Janvier et al. 2021). M. Janvier et al. (2021) showed that the recovery phase exhibits an anisotropy in the GCR flux that is consistent with the spatial gradient of the CR density being filled in from the ambient heliosphere, while I. G. Usoskin et al. (2008) demonstrated that the recovery timescale depends on particle energy, with higher energy CRs recovering faster due to their larger diffusion coefficients.

Our study shows that the rate of CR decrease varies across different ICME substructures. In several events, ICMEs or merged structures exhibit decline rates comparable to or exceeding those of the sheath region, indicating that strong magnetic compression in interacting CMEs plays an important role in rapid CR modulation. From Table 2, the dominant contributor to the FD amplitude also varies among events: ICME1 in two cases, ICME2 in three, merged ICME in two, and the IR in one. This variability suggests that no single ICME substructure consistently controls the FD, and that the relative contributions depend on the magnetic and plasma properties of the interacting CMEs.

Based on the analysis of the eight events, the CR decrease is observed to occur predominantly within intervals of enhanced magnetic field, typically beginning near the ICME shock–sheath region or just ahead of the shock, and reaching its minimum within the ICME or the IR formed due to CME–CME interaction. The onset of the CR decrease frequently coincides with enhancements in solar wind density and speed, and occasionally temperature, in the shock–sheath or leading ICME region, suggesting that these parameters may contribute to the initial drop. However,

Downloaded from academic.oup.com/mnras/article/552/1/stag1664/8785133 by Indian Institute of Astrophysics user on 19 October 2026

these plasma parameters do not consistently track the entire CR depression.

We further examined whether the eight events themselves show any systematic patterns related to their interaction configuration. Specifically, we considered whether the two CMEs merged into a single indistinguishable ejecta or remained as separate, identifiable structures, whether an IR was present, and the heliocentric distance at which the interaction occurred. In the two merged events (Events 1 and 3), the B peak–FD minimum lag is 6 and 5 h, respectively, close to the range typically reported for sheath-dominated, cross-field diffusion in isolated ICMEs (K. P. Arunbabu et al. 2015). The longest lag in our sample (17 h, Event 4) occurs in a separate structure event. In this event, the FD dominant ICME2 arrives well after the weaker ICME1 and its sheath. This suggests that widely separated successive substructures can extend the effective B–FD lag beyond typical values, but this result is based on a single event and should be treated as illustrative rather than general. We also compared the interaction distance from the Sun (as reported in the case studies cited in Section 2 with the FD onset lead time relative to shock arrival (Table 1). Events in which the interacting CMEs collided relatively close to the Sun (Event 7, $\sim$35 $R_{\odot}$; Event 8, interaction reported close to the Sun) show among the largest FD onset lead times in our sample (5 and 11 h, respectively), whereas events in which the interaction occurred farther out, closer to 1 au (Event 3, $\sim$145 $R_{\odot}$; Event 6, $\sim$215 $R_{\odot}$), show smaller lead times (2 and 1 h, respectively). This is consistent with the physical expectation that an earlier interaction allows more time for the compressed and merged structure to precondition the upstream medium before the primary shock arrives at 1 au, extending the region over which CR modulation can begin. We emphasize that with only eight events, this trend is suggestive rather than statistically robust, and a larger sample spanning a range of interaction distances would be required to confirm it. No clear relationship was found between the merged/separate distinction, or the presence of an IR, and the total FD amplitude, given the scatter present in our small sample.

Overall, the interacting ICME events analyzed here exhibit multistep FD profiles arising from the sequential passage of multiple substructures (sheath, ICME1, ICME2, IR), which is a structural feature not present in isolated single-ejecta events. The FD amplitudes measured here (2.5–5.8 per cent) fall within or above the ranges reported for isolated ICMEs (I. G. Richardson & H. V. Cane 2011; M. Janvier et al. 2021), and the recovery durations (2–4 d) are within the typical range for non-recurrent FDs (H. V. Cane 2000). The B peak–FD minimum lags observed in events where the B peak is in the sheath (1–6 h) are consistent with the cross-field diffusion times reported by K. P. Arunbabu et al. (2015) for isolated events, while longer lags (8–17 h) in events with multiple sequential substructures may reflect the added complexity of interacting configurations. A direct quantitative comparison with a matched sample of isolated events would be needed to establish whether interacting events produce systematically different FD characteristics in amplitude, duration, or decline rates.

The event-by-event analysis shows that no consistent trend is found regarding whether the preceding or the following ICME contributes more significantly to the FD amplitude. It appears that dominant contributing substructures (ICME1/ICME2/IR) exhibit enhancements in different plasma and magnetic parameters. In some events, the FD is mainly associated with strong magnetic field compression, whereas in others, elevated solar wind speed, density, and temperature indicate enhanced compression and/or turbulence that contribute significantly to CR modulation. These factors together determine the effectiveness of the diffusion barrier. A larger statistical sample is therefore required to determine which ICME substructure is more favorable for producing stronger FD and whether it depends on the relative magnetic field configuration of interacting CMEs, collision distance, and the nature of the CME-CME interaction.

4 CONCLUSIONS

The analysis of eight interacting CME events and their associated FDs leads to the following conclusions:

(i) All interacting ICME events produced clear non-recurrent FDs with amplitudes ranging from $\sim$2.5 per cent to $\sim$5.8 per cent. The strongest geomagnetic storm (Dst ~-223 nT) corresponds to the largest FD amplitude, although only a moderate correlation is observed between FD and Dst, indicating that they are governed by different physical processes.

(ii) The FD profiles generally exhibit multistep structures corresponding to successive substructures such as shock-sheath regions, ICME1, ICME2, merged ICMEs, and IRs. This behavior contrasts with isolated ICME events and indicates that interacting CMEs form extended and complex diffusion barriers with multiple substructures.

(iii) The FD onset relative to the interplanetary shock varies among events, with some onsets coinciding with the shock and others occurring 3–11 h earlier. This suggests that CR modulation can begin upstream of the shock in some interacting CME events. This suggests that CR modulation can act as an early indicator of approaching interplanetary shock.

(iv) Overall, the CR-decreasing phase is primarily associated with enhanced magnetic field conditions, while density and speed may play a secondary role during the onset or early phase, and temperature does not show a systematic correspondence across the events.

(v) A lag of 1–17 h ($\pm$1.4 h uncertainty) is observed between the IMF peak and FD minimum. The physical origin of this lag differs between substructures: in the sheath it reflects cross-field diffusion time (K. P. Arunbabu et al. 2015), while in the ejecta it reflects the evolving balance between perpendicular diffusion and flux-rope expansion (M. Dumbović et al. 2018). The delay between the FD minimum and the Dst minimum ranges from 0 to 8 h, reflecting the distinct physical drivers of CR modulation and geomagnetic activity.

(vi) All events exhibit recovery phases lasting 2–4 d, within the range typically reported for non-recurrent ICME-driven FDs (H. V. Cane 2000; M. Janvier et al. 2021). No consistent trend is found regarding whether the preceding or following ICME contributes the largest CR decrease, indicating that the relative contributions depend on the magnetic and plasma properties of individual substructures in each event. A larger statistical sample is needed to determine whether systematic differences exist between interacting and isolated ICME-driven FDs.

ACKNOWLEDGEMENTS

This work and the authors are supported by the India-Uzbekistan joint projects INT-UZBEK/P-15 and UZB-IND-2021-95. The major part of the work was carried out during the visit of ZM to Udaipur Solar Observatory, Udaipur, in 2023 August. The visit was funded by the project grant.

Downloaded from academic.oup.com/mnras/article/552/1/stag1664/8785133 by Indian Institute of Astrophysics user on 19 October 2026

DATA AVAILABILITY

The authors would like to acknowledge the use of the Richardson-Cane catalogue of ICMEs and CDAWeb for providing the *in situ* observations of solar wind at 1 au for the selected ICMEs.

REFERENCES

Arunbabu K. P. et al., 2013s, A&A, 555, A139
Arunbabu K. P. et al., 2015, A&A, 580, A41
Badruddin B., Aslam O. P. M., Derouich M., Asiri H., Kudela K., 2019, Space Weather, 17, 487
Belov A., Eroshenko E., Yanke V., Oleneva V., Abunin A., Abunina M., Papaioannou A., Mavromichalaki H., 2018, Sol. Phys., 293, 68
Bhaskar A., Subramanian P., Vichare G., 2016, ApJ, 828, 104
Brueckner G. E. et al., 1995, Sol. Phys., 162, 357
Burlaga L., Sittler E., Mariani F., Schwenn R., 1981, J. Geophys. Res., 86, 6673
Cane H. V., 2000, Space Sci. Rev., 93, 55
Cane H. V., Richardson I. G., von Rosenvinge T. T., Wibberenz G., 1994, J. Geophys. Res., 99, 21429
Davies E. E., Winslow R. M., Lawrence D. J., 2023a, ApJ, 943, 83
Davies E. E., Scolini C., Winslow R. M., Jordan A. P., Möstl C., 2023b, ApJ, 959, 133
Dumbović M., Heber B., Vršnak B., Temmer M., Kirin A., 2018, ApJ, 860, 71
Dumbović M. et al., 2020, Sol. Phys., 295, 104
Dumbović M., Kramarić L., Benko I., Heber B., Vršnak B., 2024, A&A, 683, A168
Forbush S. E., 1937, Phys. Rev., 51, 1108
Freiherr von Forstner J. L. et al., 2020, J. Geophys. Res. (Space Phys.), 125, e27662
Janvier M., Démoulin P., Guo J., Dasso S., Regnault F., Topsi-Moutesidou S., Gutierrez C., Perri B., 2021, ApJ, 922, 216
Jordan A. P., Spence H. E., Blake J. B., Shaul D. N. A., 2011, J. Geophys. Res. (Space Phys.), 116, A11103
Kane R. P., 2010, Ann. Geophys., 28, 479
Khuntia S., Mishra W., Agarwal A., 2025, A&A, 698, A79
Kilpua E., Koskinen H. E. J., Pulkkinen T. I., 2017, Living Rev. Sol. Phys., 14, 5
King J. H., Papitashvili N. E., 2005, J. Geophys. Res. (Space Phys.), 110, A02104
Kinoshita G. et al., 2026, ApJ, 997, 2
Lara A., Borgazzi A., Guennam E., Niembro T., Arunbabu K. P., 2024, J. Geophys. Res. (Space Phys.), 129, e2024JA032478
Liu Y. D., Luhmann J. G., Lugaz N., Möstl C., Davies J. A., Bale S. D., Lin R. P., 2013, ApJ, 769, 45
Liu Y. D., Hu H., Wang R., Yang Z., Zhu B., Liu Y. A., Luhmann J. G., Richardson J. D., 2015, ApJ, 809, L34
Lugaz N., Farrugia C. J., Davies J. A., Möstl C., Davis C. J., Roussev I. I., Temmer M., 2012, ApJ, 759, 68
Maričić D. et al., 2014, Sol. Phys., 289, 351
Masías-Meza J. J., Dasso S., Démoulin P., Rodriguez L., Janvier M., 2016, A&A, 592, A118
Mishra W., Srivastava N., 2014, ApJ, 794, 64
Mishra W., Srivastava N., Singh T., 2015a, J. Geophys. Res. (Space Phys.), 120, 10,221
Mishra W., Srivastava N., Chakrabarty D., 2015b, Sol. Phys., 290, 527
Mishra W., Wang Y., Srivastava N., 2016, ApJ, 831, 99
Mishra W., Wang Y., Srivastava N., Shen C., 2017, ApJS, 232, 5
Mishra W., Dave K., Srivastava N., Teriaca L., 2021, MNRAS, 506, 1186
Papaioannou A., Belov A., Abunina M., Eroshenko E., Abunin A., Anastasiadis A., Patsourakos S., Mavromichalaki H., 2020, ApJ, 890, 101
Richardson I., Cane H., 2024, Near-Earth interplanetary coronal mass ejections since January 1996. Harvard Dataverse, Vol. 297, p. 139, https://doi.org/10.7910/DVN/C2MHTH
Richardson I. G., Cane H. V., 2010, Sol. Phys., 264, 189
Richardson I. G., Cane H. V., 2011, Sol. Phys., 270, 609
Shlyk N. S., Belov A. V., Abunina M. A., Abunin A. A., Oleneva V. A., Yanke V. G., 2022, MNRAS, 511, 5897
Simpson J. A., 1954, Phys. Rev., 94, 426
Srivastava N., Mishra W., Chakrabarty D., 2018, Sol. Phys., 293, 5
Temmer M., Veronig A. M., Peinhart V., Vršnak B., 2014, ApJ, 785, 85
Temmer M. et al., 2023, preprint (arXiv:2308.04851), https://doi.org/10.48550/arXiv.2308.04851
Usoskin I. G., Braun I., Gladysheva O. G., HöRandel J. R., JäMséN T., Kovaltsov G. A., Starodubtsev S. A., 2008, J. Geophys. Res. (Space Phys.), 113, A07102
Wibberenz G., Le Roux J. A., Potgieter M. S., Bieber J. W., 1998, Space Sci. Rev., 83, 309

This paper has been typeset from a TEX/LATEX file prepared by the author.

Downloaded from academic.oup.com/mnras/article/552/1/stag1664/8785133 by Indian Institute of Astrophysics user on 19 October 2026

© The Author(s) 2026.
Published by Oxford University Press on behalf of Royal Astronomical Society. This is an Open Access article distributed under the terms of the Creative Commons Attribution License (https://creativecommons.org/licenses/by/4.0/), which permits unrestricted reuse, distribution, and reproduction in any medium, provided the original work is properly cited.